Mineralogical Magazine (2026), **90**, 673–660
doi:10.1180/mgm.2025.10144

CAMBRIDGE UNIVERSITY PRESS

Article

Kenomicrolite, $\square_2Ta_2O_4(OH)_2\square$, the first vacancy-dominated pyrochlore-supergroup mineral from the Volta Grande pegmatite, Nazareno, Minas Gerais, Brazil

Alice Taddei[1], Daniel Atencio[2] and Luca Bindi[1]

[1]Dipartimento di Scienze della Terra, Università degli Studi di Firenze, Firenze, Italy and [2]Departamento de Mineralogia e Geotectônica, Instituto de Geociências, Universidade de São Paulo, São Paulo, SP, Brazil

Abstract

Kenomicrolite (IMA 2024-097), ideally $\square_2Ta_2[O_4(OH)_2]\square$, (where $\square$ = vacancy) is a newly approved mineral species from the Volta Grande pegmatite, Nazareno, Minas Gerais, Brazil. It is the first member of the pyrochlore supergroup to exhibit dominant vacancies at both *A* and *Y* sites and a Ta-dominated *B* site, making it a tantalum oxyhydroxide. It occurs as an accessory mineral within a microlite group assemblage, probably of secondary origin via weathering-induced leaching and hydration of fluorcalciomicrolite. Kenomicrolite appears as pale orange, transparent, isotropic octahedral crystals up to 200 μm in size, with a calculated density of 5.599 g·cm^{-3} and calculated refractive index of 1.880. Its empirical formula is $^{A}(\square_{1.61}Ba_{0.29}Ce_{0.03}U_{0.03}Pb_{0.02}Mn_{0.01}Sr_{0.01})_{\Sigma2.00}{}^{B}(Ta_{1.74}Nb_{0.11}Sn_{0.08}Si_{0.05}Al_{0.01}Ti_{0.01})_{\Sigma2.00}{}^{X}[O_{4.65}(OH)_{1.35}]_{\Sigma6.00}{}^{Y}[\square_{0.57}(H_2O)_{0.35}F_{0.07}K_{0.01}]_{\Sigma1.00}$. The structure has been determined by single-crystal X-ray diffraction in the $Fd\bar{3}m$ space group type, with a = 10.5911(6) Å. Spectroscopic analyses confirmed the presence of structural water primarily at the *Y* site. Ion-exchange experiments in Tl^+-rich solutions showed minimal incorporation (~0.19 Tl^+ pfu), highlighting limited ion-exchange capacity due to vacancy-dominated tunnel sites. The structural stability and low hydration make kenomicrolite an important end-member for understanding vacancy-rich pyrochlore systems and their constraints on ion incorporation mechanisms.

Keywords: kenomicrolite; new mineral; Volta Grande pegmatite; Minas Gerais; pyrochlore supergroup; microlite group; ion-exchange properties; thallium

(Received 7 July 2025; revised 18 August 2025; accepted 18 August 2025; Accepted Manuscript published online: 22 August 2025)

Introduction

Kenomicrolite, ideally $\square_2Ta_2[O_4(OH)_2]\square$, is a new mineral (IMA 2024-097) from the Volta Grande pegmatite, Nazareno, Minas Gerais, Brazil. The general formula of pyrochlore-supergroup minerals is $A_{2-m}B_2X_{6-w}Y_{1-n}$, where m (0–1.7), w (0–0.7) and n (0–1) represent the number of vacancies at each site (Lumpkin and Ewing, 1995). *A* refers to a site with eight-fold coordination that can accommodate Na, Ca, Sr, Ba, Pb^{2+}, Sn^{2+}, Sb^{3+}, Y^{3+}, U^{4+}, H_2O, Sc, REE^{3+}, Ag, Mn^{2+}, Fe^{2+}, Cr, Th or is partially vacant. The *B* site has six-fold coordination and hosts high-field strength elements such as Ta, Nb, Ti, Sb^{5+}, W, V^{5+}, Sn^{4+}, Zr, Hf, Fe^{3+}, Mg, Al, P and Si. The *X* site mainly contains O and subordinate OH, F and/or vacancies, and the *Y* site is typically occupied by OH, F, O, $\square$ (vacancy), H_2O or large cations such as K^+, Cs^+ and Rb^+ (Ercit *et al.*, 1993). Kenomicrolite is the first mineral belonging to the pyrochlore supergroup having both *A* and *Y* dominated by vacancy and the *B* site dominated by Ta, making it, ideally, a tantalum oxyhydroxide. Kenomicrolite was allegedly observed at the María Elena pegmatite, Sierra de San Luis, Argentina (Galliski *et al.*, 2021) and at the São João Del Rei Pegmatite Province, Minas Gerais, Brazil (Menezes da Silva, 2018; Alves *et al.*, 2021), where the present sample was also found; however, none of those authors provided exhaustive data. The chosen name complies with the currently approved nomenclature system for pyrochlore-supergroup minerals (yaroot rule, Atencio *et al.*, 2010; Atencio, 2021). The root name is microlite, as Ta dominates *B*; both tunnel sites (*A* and *Y*) are dominated by structural vacancy, thus the prefix 'keno-'. Where the first and second prefixes are equal, then only one prefix is applied. The recommended mineral symbol is Kmic (Warr, 2021).

Holotype material, consisting of two small kenomicrolite crystals, is deposited in the mineralogical collection of the Museo di Storia Naturale, Sezione di Mineralogia e Litologia, Università di Firenze, Firenze (Italy), under catalogue number MSN-MIN 3747-I.

Corresponding author: Luca Bindi; Email: luca.bindi@unifi.it
Associate Editor: Giancarlo Della Ventura
Cite this article: Taddei A., Atencio D. and Bindi L. (2026) Kenomicrolite, $\square_2Ta_2O_4(OH)_2\square$, the first vacancy-dominated pyrochlore-supergroup mineral from the Volta Grande pegmatite, Nazareno, Minas Gerais, Brazil. *Mineralogical Magazine* **90**, 653–660. https://doi.org/10.1180/mgm.2025.10144

Kenomicrolite was discovered during a systematic study of hydrokenomicrolite crystals with the aim of investigating their ion-exchange capacity. Indeed, pyrochlore minerals and their synthetic analogues exhibit significant ion-exchange properties (Möller *et al.*, 2002; Zoppi, 2004; Han *et al.*, 2014; Taddei *et al.*, 2024), due to the easy leachability of the *A* and *Y* species, especially when they are large and have low charge (K^+, Cs^+, Tl^+, etc.) and/or highly mobile (H_2O). This property has significant environmental implications, as pyrochlores can represent promising candidates as sinks for toxic metals such as Tl or Pb. The number of possible exchangers at the tunnel sites in kenomicrolite is very limited, given that both sites are vacancy-dominated, and they are mainly represented by aqueous species (H_2O + OH^- or H_3O^+); for this reason, kenomicrolite should not be regarded as the best choice for heavy metals immobilisation. Nonetheless, the incorporation mechanism involving Tl^+ in the structure of kenomicrolite was hereby investigated in order to have more insights on the limits of critical features of the crystal structure of pyrochlore minerals.

Occurrence

The new mineral (Fig. 1) occurs at the Volta Grande pegmatite (21°10′08.6′′S, 44°36′01.3′′W), Nazareno, Minas Gerais, Brazil as an accessory phase. The pegmatite belongs to the Sn-Ta-rich São João del Rei Pegmatite Province (Heinrich, 1964; Lagache and Quéméneur, 1997). The Volta Grande granitic pegmatite is associated with Transamazonian granites (Early Proterozoic) hosted by the Archean greenstone belt of the Rio das Mortes Valley, which is situated at the southern border of the São Francisco Craton, in Minas Gerais, Brazil (Lagache and Quéméneur, 1997). The pegmatite bodies, which are usually large (up to 1200 m × 40 m), show a dominant intermediate zone containing spodumene, microcline, albite and quartz, with an irregular border of an aplitic facies surrounded by an extensive metasomatic aureole with 'zinnwaldite', phlogopite and holmquistite. The spodumene-rich core zone is continuous or segmented and also contains lenses of 'lepidolite'. The main rock type that hosts the pegmatite is an amphibole schist. This pegmatite is characterized by high Rb and Li contents (Lagache and Quéméneur, 1997). The paragenetic position of the mineral could not be determined, as it was found in a large octahedral fragment collected in a heavy mineral concentrate (see Andrade *et al.*, 2013a). The octahedral fragments are formed by an association of kenomicrolite and hydrokenomicrolite together with Na-rich fluorcalciomicrolite, pointing to a possible secondary origin of kenomicrolite. The leaching of Ca, Na and F from primary fluorcalciomicrolite can be a consequence of weathering (Lumpkin and Ewing, 1992), followed by a subsequent limited uptake of locally enriched cations (in this case, Ba, Ce, U, Pb, Mn, Sr) as well as water molecules. Depending on the extent of the hydration process, either hydrokenomicrolite or kenomicrolite can form this way.

Other associated minerals within the pegmatite are albite, fluorapatite, beryl, bityite, cassiterite, epidote, fluorite, 'garnet', gahnite, hydroxycalciomicrolite, 'lepidolite', magnetite, microcline, monazite-(Ce), muscovite, quartz, rutile, spodumene, tantalite-(Mn), 'tourmaline' and zircon.

Nazareno is the type locality for hydrokenomicrolite (Andrade *et al.*, 2013a), fluorcalciomicrolite (Andrade *et al.*, 2013b), hydroxycalciomicrolite (Andrade *et al.*, 2017) and oxycalciomicrolite (Menezes da Silva *et al.*, 2020).

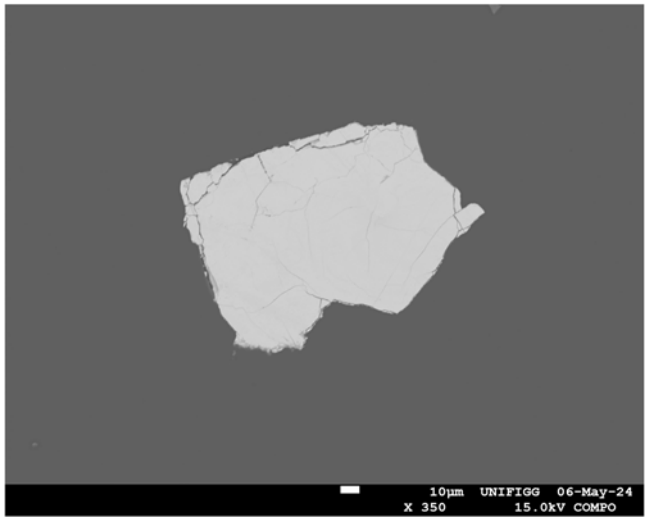

Figure 1. Back-scattered electron image of the kenomicrolite fragment investigated.

Appearance, physical and optical properties

Kenomicrolite forms small areas in hydrokenomicrolite euhedral octahedral crystals, probably pseudomorphs after fluorcalciomicrolite, up to 200 µm in size (Fig. 1). The colour is pale orange, with a white streak; the crystals are transparent with an adamantine to resinous lustre, and they have an altered appearance, scarcely distinguishable from hydrokenomicrolite grains. Kenomicrolite is brittle and displays a conchoidal fracture, while no cleavage or parting are observed; the estimated Mohs hardness is 6. It shows no fluorescence under UV light. The density was not measured because of the size of available grains. The calculated value of 5.599 g·cm^{-3} was obtained on the basis of the empirical chemical formula and the unit-cell volume obtained from single-crystal X-ray diffraction data (see below).

Kenomicrolite is isotropic, with n_{calc} = 1.880 (from the Gladstone–Dale relationship for the empirical formula; Mandarino, 1981). Other optical data were not collected given the availability of only two small crystals.

Chemical data

Chemical analyses were carried out on the fragment from which the crystal used for the structural study was extracted, using a Jeol JXA-8230 electron microprobe (EMPA; tungsten cathode) in wavelength dispersion mode (WDS) at 15 kV acceleration voltage, 10 nA beam current and 2 µm beam size. The total number of spot analyses on the investigated crystal was 5. Based on standard deviation values, the crystal was found to be homogeneous (with slightly variable degrees of hydration from point to point). The occurrence of H_2O was confirmed by infrared spectroscopy and was calculated in accordance with the results of the crystal structure refinement; a direct measurement was prevented by dearth of material. All Fe was assumed to be Fe^{3+} and all Sn to be Sn^{4+}. Th and Zr were measured but were found to be below the detection limit (0.01 wt.%). Mean analytical results are given in Table 1.

The empirical formula, calculated on the basis of 2 *B* cations pfu, can be written as $^{A}(\square_{1.61}Ba_{0.29}Ce_{0.03}U_{0.03}Pb_{0.02}Mn_{0.01}Sr_{0.01})_{\Sigma 2.00}$ $^{B}(Ta_{1.74}Nb_{0.11}Sn_{0.08}Si_{0.05}Al_{0.01}Ti_{0.01})_{\Sigma 2.00}$ $^{X}[O_{4.65}(OH)_{1.35}]_{\Sigma 6.00}$

Table 1. Analytical data (wt.%) for kenomicrolite

Constituent	wt.%	Range	S.D.	Probe standard
Nb_2O_5	2.88	2.15–3.05	0.44	Nb metal
Sb_2O_5	0.02	0.00–0.04	0.04	Sb metal
Ta_2O_5	77.63	76.00–78.46	1.08	Ta metal
SiO_2	0.66	0.20–1.27	0.43	albite
TiO_2	0.17	0.00–0.24	0.10	ilmenite
SnO_2	2.48	1.89–2.76	0.38	cassiterite
UO_2	1.89	1.75–1.99	0.09	U metal
Al_2O_3	0.13	0.04–0.28	0.10	plagioclase
Fe_2O_3	0.02	0.00–0.09	0.04	ilmenite
La_2O_3	0.02	0.00–0.12	0.06	monazite
Ce_2O_3	1.00	0.96–1.08	0.04	monazite
CaO	0.01	0.00–0.05	0.02	diopside
MnO	0.19	0.00–0.28	0.12	bustamite
SrO	0.18	0.08–0.25	0.08	celestite
BaO	9.07	8.16–10.43	0.89	baryte
PbO	1.07	0.53–1.46	0.38	crocoite
Na_2O	0.01	0.00–0.02	0.01	albite
K_2O	0.10	0.08–0.14	0.02	sanidine
Tl_2O	0.14	0.00–0.49	0.20	lorandite
F	0.27	0.15–0.46	0.16	fluorite
H_2O*	3.10			
O=F	−0.11			
TOT	100.93			

*Calculated from structural formula – the value in atoms per formula unit (apfu; 1.35 at *X* + 0.35 at *Y*) was converted to H_2O wt.% as follows: the value in apfu was divided by the normalization parameter (ΣB = 2) and then multiplied by two to obtain H_2O mol.%. The latter was then multiplied by the molecular weight of H_2O, resulting in H_2O wt.%. S.D. – standard deviation.

$^{Y}[\square_{0.57}(H_2O)_{0.35}F_{0.07}K_{0.01}]_{\Sigma 1.00}$ (where pfu = per formula unit). The ideal chemical formula of kenomicrolite is thus $\square_2Ta_2[O_4(OH)_2]\square$, which requires Ta_2O_5 96.09, H_2O 3.91, total 100.00 wt.%.

X-ray diffraction

Single-crystal data

Single-crystal X-ray diffraction (SC-XRD) investigations were performed on two single crystals (labelled KM and KM2) extracted from the fragment in Fig. 1, with a Bruker D8 Venture diffractometer equipped with a Photon III detector. Unit-cell parameters and intensity data were collected using graphite-monochromatized Mo*K*α radiation (λ = 0.71073 Å). Crystal data and experimental conditions are listed in Table 2. Intensity data were integrated by means of the *APEX5* software suite (Bruker, 2023) and corrected for Lorentz-polarization effects and for absorption (multi-scan method – *SADABS*). Given the close relation to other cubic pyrochlore minerals, the structure was refined in the space group $Fd\bar{3}m$ (origin choice 2) using the program *SHELXL* (Sheldrick, 2015). The refinement was carried out starting from the atomic coordinates reported for hydrokenomicrolite (Andrade *et al.*, 2013a) for *A, B, X* and *Y*. All these sites are located at special Wyckoff positions: *A* = 16*d*, *B* = 16*c*, *X* = 48*f* and *Y* = 8*b*. Site occupancy factors (s.o.f.s) were refined using the following scattering curves for neutral atoms (from the *International Tables for Crystallography*; Wilson, 1992): Ba *vs* □ (*A*), Ta *vs* Nb (*B*), O (*X*), O *vs* □ (*Y*). The s.o.f. value of the *B* site was fixed to EMPA values. Final coordinates and equivalent isotropic displacement parameters are given in Table 3, while selected interatomic distances are reported in Table 4. More details are included in the crystallographic information files (CIFs), available as supplementary material.

The bond valence sums (BVSs), calculated for the KM crystal considering the site populations as obtained from microprobe data and using the parameters given by Brese and O'Keeffe (1991), are reported in Table 5; lastly, Table 6 contains a comparison between the electron numbers calculated from microprobe data and those obtained from the structural model of sample KM.

Powder diffraction data

Powder X-ray diffraction data were collected using a Gandolfi-like experiment on KM, using Cu*K*α radiation (λ = 1.54178 Å). Unit-cell parameters refined from powder data (space group $Fd\bar{3}m$) are a = 10.5628(3) Å and V = 1178.52(10) Å^3. A comparison of the measured powder diffraction data and those calculated from the structural model is given in Table 7.

Infrared spectroscopy

Fourier-transform infrared spectroscopy (FTIR) data were collected in transmission mode by placing the KM crystal on an IR-transparent BaF_2 plate. The analyses were carried out by means of a Nicolet RaptIR microscope attached to a Nicolet iS50 FTIR spectrometer (Thermo Fisher), equipped with a Polaris IR source, KBr beam splitter and a LN2 MCT detector. The spectrum (Fig. 2) was collected adjusting the aperture size to that of the crystal; sixty-four scans were averaged, with a spectral range between 5000 and 650 cm^{-1} and a resolution of 4 cm^{-1}.

Spectral features are observed at 893sh, 1009sh, 1077, 1236w, 1442, 1644, ~2700 to ~3600, 3730w, 4023w, 4469w cm^{-1}. The large band occurring between 2700 and 3600 cm^{-1} and the small peak at 3730 cm^{-1} can be interpreted as due to O–H stretching vibrations, while H–O–H bending vibrations can be observed at 1644 cm^{-1}. A comparison with the spectrum of a hydrokenomicrolite single crystal (Fig. 3), collected under identical instrumental conditions, shows a weaker H_2O bending mode band in kenomicrolite. This agrees with the lower amount of H_2O groups in kenomicrolite compared to hydrokenomicrolite. Bands between 840 and 1240 cm^{-1} are probably related to Ta···O–H bending vibrations (Andrade *et al.*, 2013a). Lastly, the weak bands above 4000 cm^{-1} can be ascribed to H_2O combination modes.

Imbibition experiments in a Tl^+-rich solution

KM2 was soaked for 5 days in a thallium(I) formate-deionised water solution having a concentration of 1M Tl^+. SC-XRD data were collected before and after the imbibition experiment (Tables 2–3) as described above.

Discussion

Crystal chemistry of kenomicrolite

The crystal structure of kenomicrolite (Fig. 4) is topologically identical to that of other pyrochlore minerals crystallising in the space group type $Fd\bar{3}m$, showing a framework of corner-linked BX_6 octahedra that forms tunnels running parallel to [110]. The tunnels host the interstitial *A* and *Y* sites. In kenomicrolite, Ta is dominant at the *B* site, along with minor Nb, Sn, Si, Al and Ti. The *A* site has been found mainly vacant, having Ba as the most abundant cation

Table 2. Crystal data, experimental details and refinement details for kenomicrolite and Tl-treated kenomicrolite

	KM	KM2	KM2_Tl
Crystal data			
Crystal size (mm)	0.070 × 0.070 × 0.050	0.120 × 0.110 × 0.100	0.120 × 0.110 × 0.100
Cell setting, space group	Cubic, $Fd\bar{3}m$	Cubic, $Fd\bar{3}m$	Cubic, $Fd\bar{3}m$
a (Å)	10.5911(6)	10.5707(17)	10.574(3)
V (Å^3)	1188.0(2)	1181.2(6)	1182.3(10)
Z	8	8	8
Data-collection details			
Radiation, wavelength (Å)	Mo$K\alpha$, λ = 0.71073	Mo$K\alpha$, λ = 0.71073	Mo$K\alpha$, λ = 0.71073
Temperature (K)	298	298	298
$^\circ 2\theta_{max}$	63.79	63.93	63.91
Measured reflections	4155	1955	1571
Unique reflections	125	125	125
Reflections with $F_o > 4\sigma(F_o)$	95	93	93
R_{int} (%)	7.24	7.56	7.73
Range of h, k, l	$-15 \le h \le 15$ $-15 \le k \le 15$ $-15 \le l \le 15$	$-13 \le h \le 15$ $-13 \le k \le 15$ $-15 \le l \le 13$	$-15 \le h \le 12$ $-11 \le k \le 13$ $-10 \le l \le 15$
Refinement details			
R [$F_o > 4\sigma(F_o)$]	0.0291	0.0447	0.0648
R (all data)	0.0420	0.0621	0.0792
GoF	1.194	1.278	1.161
Number of least-square parameters	12	12	13

Table 3. Atomic coordinates, Wyckoff positions, site occupancy factors (s.o.f.) and thermal parameters (Å^2) for kenomicrolite and Tl-treated kenomicrolite

Site	Wyckoff	s.o.f.	x/a	y/b	z/c	U_{eq}
KM						
A	16*d*	$Ba_{0.197(9)}\square_{0.803}$	½	½	½	0.013(2)
*B**	16*c*	$Ta_{0.85}Nb_{0.15}$	0	0	0	0.0193(4)
X	48*f*	$O_{1.00}$	0.3130(9)	⅛	⅛	0.0208(17)
Y	8*b*	$O_{0.45(11)}\square_{0.55}$	⅜	⅜	⅜	0.07(4)**
KM2						
A	16*d*	$Ba_{0.193(17)}\square_{0.807}$	½	½	½	0.013(4)
*B**	16*c*	$Ta_{0.85}Nb_{0.15}$	0	0	0	0.0204(7)
X	48*f*	$O_{1.00}$	0.3145(16)	⅛	⅛	0.026(3)
Y	8*b*	$O_{0.22(12)}\square_{0.78}$	⅜	⅜	⅜	0.02(4)
KM2_Tl						
A	16*d*	$Ba_{0.32(4)}\square_{0.68}$	½	½	½	0.040(6)
*B**	16*c*	$Ta_{0.85}Nb_{0.15}$	0	0	0	0.0309(16)
X	48*f*	$O_{1.00}$	0.315(2)	⅛	⅛	0.037(5)
Y	8*b*	$O_{0.36(18)}\square_{0.64}$	⅜	⅜	⅜	0.04(5)**

*The site occupation factors for the *B* site have been fixed to the EMPA values.
**U_{iso}.

Table 4. Selected interatomic distances (Å) and angles (°) for kenomicrolite and Tl-treated kenomicrolite

	KM	KM2	KM2_Tl
A–*X* (×6)	2.725(7)	2.707(12)	2.705(18)
A–*Y* (×2)	2.2930(1)	2.2886(4)	2.2894(7)
<*A*–O>	2.617	2.602	2.601
B–*X* (×6)	1.988(3)	1.990(6)	1.992(8)
X–*B*–*X*	90.2(4)	90.9(7)	91.0(9)
X–*B*–*X*´	89.8(4)	89.1(7)	89.0(9)
B–*X*–*B*	140.8(5)	139.8(9)	139.6(13)
B–*X*–*A*	104.13(15)	104.4(3)	104.4(4)
A–*X*–*A*	86.8(3)	87.3(5)	87.4(7)

Table 5. Bond valence sums (BVS) for kenomicrolite (sample KM), calculated considering populations as calculated using EMPA (1) and the structure refinement (2)

	A	B	SUM (1)	SUM (2)
X	$^{\downarrow x6\rightarrow x2}$0.053	$^{\downarrow x6\rightarrow x2}$0.815	1.74*	
Y	$^{\downarrow x2\rightarrow x4}$0.069		0.28	
SUM (1)	0.46	4.89		
Expected value	0.44	4.92		
X	$^{\downarrow x6\rightarrow x2}$0.060	$^{\downarrow x6\rightarrow x2}$0.829		1.78*
Y	$^{\downarrow x2\rightarrow x4}$0.087			0.35
SUM (2)	0.53	4.97		
Expected value	0.44	4.92		

*In agreement with the partial substitution of O for OH at *X*.

(0.29 atoms per formula unit) accompanied by minor ($\le$ 0.03 apfu) Ce, U^{4+}, Pb^{2+}, Mn^{2+} and Sr. The total cationic population at this site is 0.39 apfu. In both crystals (KM and KM2), no H_2O groups were observed at *A*, as the refined electron number (11.0 e^- and 10.8 e^-, respectively) matches well that calculated from microprobe data (11.5 e^-), even without additional water. The *Y* site was also found to be dominated by structural vacancy: the number of electrons refined at this site was 3.6 e^- for KM. Taking into account the contribution of minor F + K (~0.8 e^-), the remaining 2.8 e^- were assigned to O, corresponding to 0.35 H_2O pfu (the presence of which was confirmed by infrared spectroscopic analyses). For KM2, the number of electrons refined at *Y* was even lower, 1.8 e^-, yielding 0.13 H_2O pfu; this discrepancy can be explained considering the slight difference in totals for the different spots, ranging from 96.24 wt.% up to 99.08 wt.% (mean 97.84 wt.%). KM2 was handpicked in a part of the fragment particularly depleted in aqueous species. Potassium was assumed at *Y* due to the relatively large ionic radius and low charge (see Ercit *et al.*, 1993, 1994). Finally,

Table 6. Comparison between the observed and calculated mean atomic number (MAN, in number of electrons per site) for kenomicrolite and Tl-treated kenomicrolite

Site	MAN_{obs}	Site occupancy	MAN_{calc}
KM			
A	11.0	$\square_{1.61}Ba_{0.29}Ce_{0.03}U_{0.03}Pb_{0.02}Mn_{0.01}Sr_{0.01}$	11.5
B	68.2*	$Ta_{1.74}Nb_{0.11}Sn_{0.08}Si_{0.05}Al_{0.01}Ti_{0.01}$	68.3
X	8.0	$O_{1.00}$	8.0
Y	3.6	$\square_{0.56}(H_2O)_{0.35}F_{0.07}K_{0.01}$	3.6
KM2			
A	10.8	$\square_{1.61}Ba_{0.29}Ce_{0.03}U_{0.03}Pb_{0.02}Mn_{0.01}Sr_{0.01}$	11.5
B	68.2*	$Ta_{1.74}Nb_{0.11}Sn_{0.08}Si_{0.05}Al_{0.01}Ti_{0.01}$	68.3
X	8.0	$O_{1.00}$	8.0
Y	1.8	$\square_{0.56}(H_2O)_{0.13}F_{0.07}K_{0.01}$	1.8
KM2_Tl			
A	17.9	$\square_{1.45}Ba_{0.29}Tl_{0.16}Ce_{0.03}U_{0.03}Pb_{0.02}Mn_{0.01}Sr_{0.01}$	11.5
B	68.2*	$Ta_{1.74}Nb_{0.11}Sn_{0.08}Si_{0.05}Al_{0.01}Ti_{0.01}$	68.3
X	8.0	$O_{1.00}$	8.0
Y	2.9	$\square_{0.89}F_{0.07}Tl_{0.03}K_{0.01}$	2.9

*Fixed occupancy. MAN_{calc} always refers to the whole kenomicrolite fragment before imbibition experiments.

Table 7. Powder X-ray diffraction data (*d* in Å) for kenomicrolite, sample KM

hkl	d_{calc}	I_{calc}	d_{meas}	I_{meas}
111	**6.1148**	**100**	**6.1**	**70**
311	**3.1933**	**52**	**3.18**	**40**
222	**3.0574**	**95**	**3.04**	**100**
400	**2.6478**	**32**	**2.637**	**28**
331	2.4298	11	2.423	8
511,333	2.0383	16	2.032	16
440	**1.8723**	**40**	**1.866**	**51**
531	1.7902	16	1.784	16
533	1.6151	7	1.611	8
622	**1.5967**	**37**	**1.593**	**40**
444	1.5287	10	1.528	9
551,711	1.4831	10	1.479	8
553,731	1.3788	10		
800	1.3239	5		
751	1.2230	3		
662	1.2149	12		
840	1.1841	11		
753	1.1625	2		
931	1.1102	3		
844	1.0809	7		
1022,666	1.0191	9		
880	0.9361	3		
973	0.8983	2		
1062	0.8951	11		
884	0.8826	7		
1151	0.8735	2		
1240	0.8373	7		

Notes: Calculated *d* values were obtained using *XPOW* (Downs *et al.*, 1993) using the atomic coordinates and site occupancies reported in Table 3 (KM line). The strongest lines are given in bold.

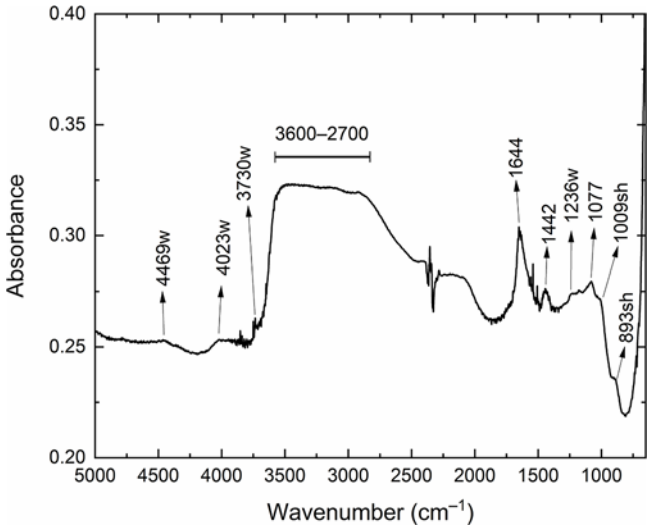

Figure 2. Transmission FTIR spectrum of kenomicrolite with labelled bands and strengths (w = weak; sh = shoulder).

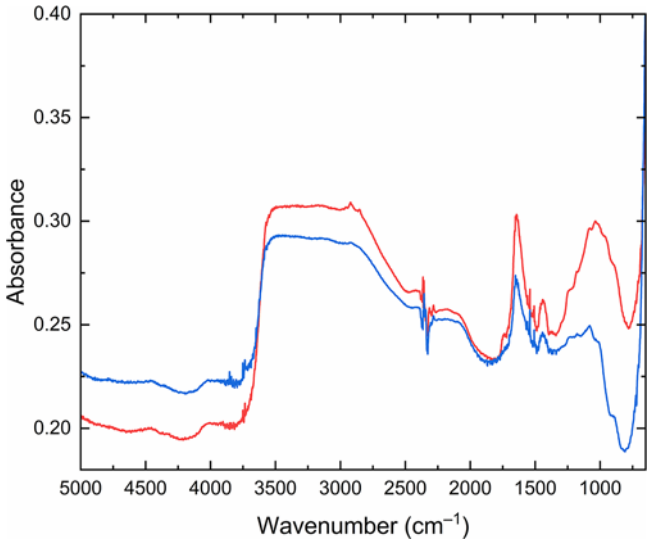

Figure 3. Comparison between the FTIR spectra of kenomicrolite (blue) and hydrokenomicrolite (red).

the charge balance was achieved by replacing O for $(OH)^-$ at the *X* site $[O_{4.65}(OH)_{1.35}]_{\Sigma 6.00}$.

Kenomicrolite displays a larger *a* parameter (10.5911(6) Å) than other zero-valent-dominant microlite-group minerals, *e.g.* hydroxykenomicrolite (*a* = 10.526(5) Å, formerly known as 'cesstibtantite'; Ercit *et al.*, 1993; Atencio *et al.*, 2010) or hydrokenomicrolite (*a* = 10.454(1) Å; Andrade *et al.*, 2013a). The latter, however, shows a unit-cell parameter refined from powder XRD data much closer to that of kenomicrolite, namely 10.5733(9) Å; furthermore, a Pb-bearing microlite mineral with the *A* site dominated by H_2O or vacancy was described by Zoppi (2004), having an *a* parameter of 10.569(1) Å. Among the hydrous pyrochlore-group minerals (thus having dominant Nb at *B*), the closest values are those of hydroxykenopyrochlore (*a* = 10.590(5) Å; Miyawaki *et al.*, 2021) and hydropyrochlore (*a* = 10.54–10.60 Å; van Wambeke, 1978; Ercit *et al.*, 1994; Philippo *et al.*, 1995; Taddei *et al.*, 2024). The numerous data available for hydropyrochlore (formerly named 'kalipyrochlore') make evident a marked variability of the unit cell in samples from the same locality, or even from the same fragment, possibly due to a certain degree of variability in composition. This could justify the slight difference observed between the unit-cell

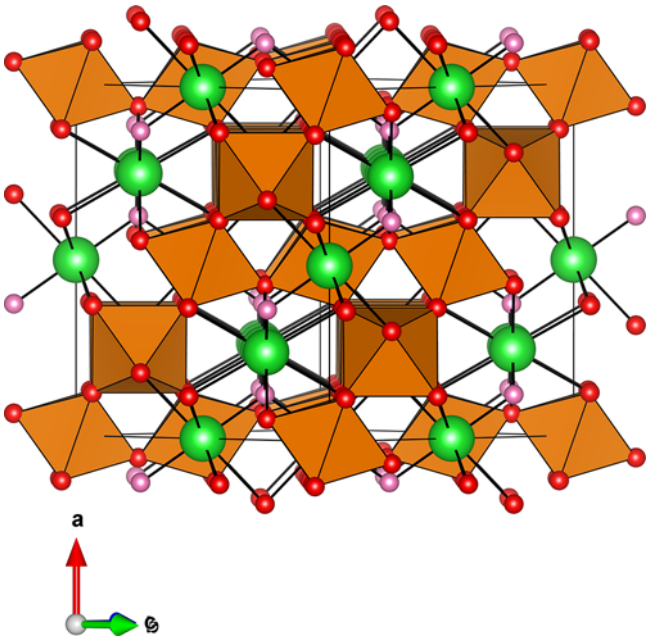

Figure 4. Kenomicrolite crystal structure approximately down [110]. Symbols: orange octahedra = *B*; green spheres = *A*; red spheres = *X*; pink spheres = *Y*. The drawing was computed using *VESTA* (Momma and Izumi, 2011).

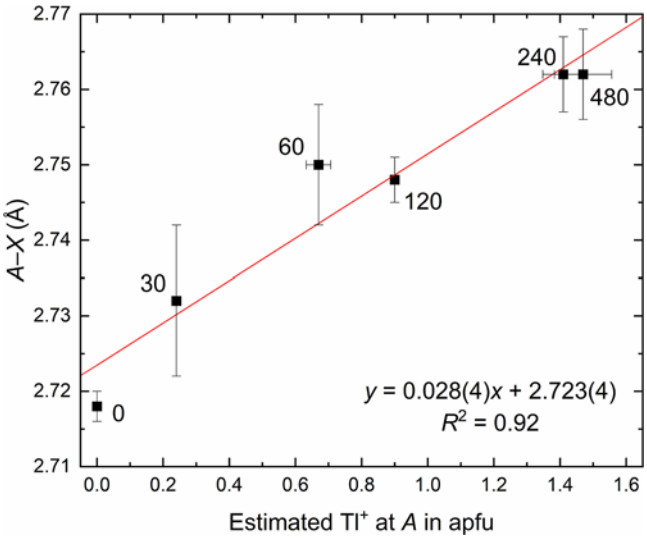

Figure 5. Linear correlation between the estimated amount of Tl^+ at the *A* site and the *A*–*X* distance, calculated using data from the hydrokenopyrochlore sample Hkpcl in Taddei and Bindi (2025). The numbers near the symbols indicate the duration (not cumulative) of the imbibition experiment in minutes; error bars that are not visible are contained within the data symbols.

parameter of KM and that of KM2, which are reasonably similar anyway.

Small deviations in the crystal structure among different pyrochlore mineral species usually occur due to positional disorder at the tunnel sites, which could give rise to split sites located in the vicinity of the ideal *A* (½, ½, ½) and *Y* (⅜, ⅜, ⅜) positions. The comparison between the kenomicrolite structure and that of hydrokenomicrolite (Andrade *et al.*, 2013a), fairly similar in composition, highlights one of the aforementioned differences: hydrokenomicrolite, containing relatively large amounts of H_2O at both tunnel sites, shows a partially occupied site near *Y* (*Y′*, 32*e*). This slight displacement from the ideal *Y* position is, in principle, necessary to maintain a physically sound distance between the oxygens when H_2O groups are simultaneously present at both *A* and *Y* (Ercit *et al.*, 1994). The distance between the two ideal positions is indeed ~2.3 Å, too short for acceptable O–O separations. In kenomicrolite this displacement does not occur, consistent with the absence of H_2O groups at *A*.

Ion-exchange properties of kenomicrolite

Pyrochlore minerals that host leachable cations (*e.g.* Na^+, K^+, etc.) or aqueous species (H_2O, H_3O^+) at the tunnel sites, can usually show enhanced ion-exchange capacity, especially for large-radius, low-charge cations (e.g. Tl^+). Taddei *et al.* (2024) pointed out two possible Tl^+ incorporation mechanisms, involving either (H_2O + OH^-) or H_3O^+. In kenomicrolite, none of the cations hosted at *A* and *Y* is monovalent (except a very minor amount of K^+ at *Y*) and the water content in the structure is small and limited to the *Y* site; therefore, a poor ion-exchange capacity is expected for this mineral. Indeed, after the imbibition experiment in a Tl-rich solution, only a slight increase in electron density was observed at both the *A* (17.9 e^-) and *Y* (2.9 e^-) sites, corresponding to an incorporation of ~0.16 Tl^+ pfu at *A* and ~0.03 Tl^+ pfu at *Y*. Considering the ion-exchange mechanisms proposed by Taddei *et al.* (2024), these values are consistent – within analytical error – with the total amount of H_2O + K^+ calculated for KM2, namely 0.14 apfu. Nevertheless, no substantial structural changes occur, in contrast with hydropyrochlore crystals subjected to the same imbibition experiments (Taddei *et al.*, 2024). In hydropyrochlore, Tl^+ incorporation induces an expansion of the unit cell due to the increase of the *A*–*X* distances, as Tl preferentially orders at the *A* site. However, hydropyrochlore can ideally host up to 1.75 apfu of water at both tunnel sites (Ercit *et al.*, 1994), making its ion-exchange capacity significantly greater; in fact, the amount of incorporated Tl^+ can reach up to 1.40 apfu. The very small quantity of Tl^+ incorporated in kenomicrolite is probably insufficient to produce measurable structural effects such as an increase of the *A*–*X* bond distances, as the observation of finer details would require better data quality (which is quite poor for these crystals, especially for KM2). Taddei and Bindi (2025) carried out a study on the kinetics of the Tl^+ incorporation reaction in hydrokenopyrochlore, highlighting an almost linear correlation between the estimated incorporated Tl at *A* and the *A*–*X* distance (Fig. 5). Given that the *A*–*X* bond length of KM2 before the treatment is shorter than that of the hydrokenopyrochlore sample studied by Taddei and Bindi (2025), it was not possible to calculate how long the *A*–*X* bond should be after the incorporation of ~0.16 Tl pfu at *A* using directly the equation in Fig. 5 [$y = 0.028(4)x + 2.723(4)$]. However, the extent of the lengthening of *A*–*X* consequent to the incorporation of the same amount of Tl for hydrokenopyrochlore (~2‰) would correspond, considering the starting distance in KM2 (2.707 Å), to an expansion up to 2.712 Å, well within the error on the *A*–*X* bond length observed for KM2_Tl (Table 4).

The hypothesis of a third reaction, based on the deprotonation of hydroxyl groups at *X* without water loss at *Y* ($^{A}Tl^+ + {}^{X}O^{2-} \rightarrow {}^{A}\square + {}^{X}OH^-$), cannot be ruled out. In hydropyrochlore, water loss is necessary due to stereochemical constraints; conversely, in kenomicrolite, which has almost-empty tunnel sites, there are no such constraints and water is not required to exit the structure to accommodate Tl^+. This mechanism appears to

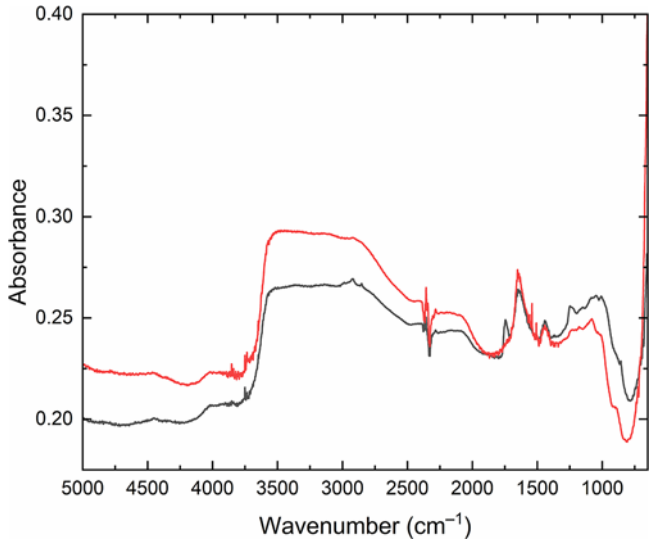

Figure 6. Comparison between the FTIR spectra of untreated kenomicrolite (red) and Tl-treated kenomicrolite (black).

be supported by FTIR data collected on KM2 after the imbibition experiment (Fig. 6). The H_2O bending-mode peak weakens slightly but remains visible, while the broad O–H stretching band decreases more significantly. The peak at 3730 cm^{-1}, possibly attributable to the stretching of OH groups at *X*, weakens considerably and becomes barely distinguishable from background noise.

In this scenario, the reaction should not be limited by the amount of OH^-, as it occurs at *X* in much greater amounts than the Tl^+ incorporated. The limited efficiency of this process, compared to those described by Taddei *et al.* (2024), may be due to other factors such as the pH of the solution, *P-T* conditions, or even the absence of water, which could facilitate H^+ loss. As for the latter factor, it seems that in pyrochlore-like structures, when hydrogen is present both as tunnel-site water and as OH groups at *X*, an intratunnel reaction may occur with an equilibrium of the type $^{B}M–^{X}OH + {}^{A+Y}H_2O \leftrightarrows {}^{B}M–O^- + H_3O^+$ (Slade *et al.*, 1996), potentially making H^+ exchange easier in highly hydrated pyrochlore minerals, where both molecular water and hydroxyl groups are largely present.

Supplementary material. The supplementary material for this article can be found at https://doi.org/10.1180/mgm.2025.10144.

Acknowledgements. The authors acknowledge CRIST, Centro di Studi per la Cristallografia Strutturale, and LaMA, Laboratorio di MicroAnalisi, both pertaining to Università degli Studi di Firenze (Italy), for X-ray diffraction and electron microprobe measurements, respectively. Two anonymous referees are thanked for their insightful comments, which improved the manuscript. DA acknowledges FAPESP (Fundação de Amparo à Pesquisa do Estado de São Paulo) for financial support (process 2024/02850-6) and CNPq (Conselho Nacional de Desenvolvimento Científico e Tecnológico) for a research productivity scholarship (process 305656/2023-6).

Competing interests. The authors declare none.

References

Alves F.E.A., Neumann R., Ávila C.A., Ferreira P.E.M., de S. Assumpção C., Carneiro M.C. and Garcia P.H.V. (2021) Mineralogical auditing of the Volta Grande Mine (SE Brazil) Sn-Ta-Nb-Li processing plant, aiming at REE recovery as by-products. *Applied Earth Science*, **130**, 198–208.

Andrade M.B., Atencio D., Chukanov N.V. and Ellena J. (2013a) Hydrokenomicrolite, (□,H_2O)Ta_2(O,OH)$_6$(H_2O), a new microlite-group mineral from Volta Grande pegmatite, Nazareno, Minas Gerais, Brazil. *American Mineralogist*, **98**, 292–296.

Andrade M.B., Atencio D., Persiano A.I.C. and Ellena J. (2013b) Fluorcalciomicrolite, (Ca,Na,□)$_2Ta_2O_6$F, a new microlite-group mineral from Volta Grande pegmatite, Nazareno, Minas Gerais, Brazil. *Mineralogical Magazine*, **77**, 2989–2996.

Andrade M.B., Yang H., Atencio D., Downs R.T., Chukanov N.V., Lemée-Cailleau M.H., Persiano A.I.C., Goeta A.E. and Ellena J. (2017) Hydroxycalciomicrolite, $Ca_{1.5}Ta_2O_6$(OH), a new member of the microlite group from Volta Grande pegmatite, Nazareno, Minas Gerais, Brazil. *Mineralogical Magazine*, **81**, 555–564.

Atencio D. (2021) Pyrochlore-supergroup minerals nomenclature: An update. *Frontiers in Chemistry*, **9**, 713368.

Atencio D., Andrade M.B., Christy A.G., Gieré R. and Kartashov P.M. (2010) The pyrochlore supergroup of minerals: nomenclature. *The Canadian Mineralogist*, **48**, 673–698.

Brese N.E. and O'Keeffe M. (1991) Bond-valence parameters for solids. *Acta Crystallographica*, **B47**, 192–197.

Bruker (2023) *APEX5 software suite*. Bruker AXS Inc., Madison, Wisconsin, USA.

Downs R.T., Bartelmehs K.L., Gibbs G.V. and Boisen M.B., Jr. (1993) Interactive software for calculating and displaying X-ray or neutron powder diffractometer patterns of crystalline materials. *American Mineralogist*, **78**, 1104–1107.

Ercit T.S., Černy P. and Hawthorne F.C. (1993) Cesstibtantite–a geologic introduction to the inverse pyrochlores. *Mineralogy and Petrology*, **48**, 235–255.

Ercit T.S., Hawthorne F.C. and Černy P. (1994) The structural chemistry of kalipyrochlore, a "hydropyrochlore". *The Canadian Mineralogist*, **32**, 415–420.

Galliski M.Á., Márquez-Zavalía M.F. and Roquet M.B. (2021) Los minerales de Nb-Ta-U de la pegmatita María Elena, Sierra de San Luis, Argentina. *Revista de la Asociación Geológica Argentina*, **78**(3), 355–367 [in Spanish].

Han Y.N., Jiao S., Xu M., Pang G. and Feng S. (2014) Solvothermal synthesis of the defect pyrochlore $KNbWO_6·H_2O$ and its application in Pb^{2+} removal. *RSC Advances*, **4**, 14357–14360.

Heinrich E.W.M. (1964) Tin-tantalum-lithium pegmatites of the São João Del Rei district, Minas Gerais, Brazil. *Economic Geology*, **59**, 982–1002.

Lagache M. and Quéméneur J. (1997) The Volta Grande pegmatites, Minas Gerais, Brazil: an example of rare-element granitic pegmatites exceptionally enriched in lithium and rubidium. *The Canadian Mineralogist*, **35**, 153–165.

Lumpkin G.R. and Ewing R.C. (1992) Geochemical alteration of pyrochlore group minerals: Microlite subgroup. *American Mineralogist*, **77**, 179–188.

Lumpkin G.R. and Ewing R.C. (1995) Geochemical alteration of pyrochlore group minerals: Pyrochlore subgroup. *American Mineralogist*, **80**, 732–743.

Mandarino J.A. (1981) The Gladstone-Dale relationship; Part IV, The compatibility concept and its application. *The Canadian Mineralogist*, **19**, 441–450.

Menezes da Silva V.H.R. (2018) *Caracterização de minerais do supergrupo do pirocloro na Província Pegmatítica de São João del Rei, Minas Gerais*. Masters thesis, Universidade Federal do Rio de Janeiro, Brazil, 113 pp. [in Portuguese].

Menezes da Silva V.H.R., Ávila C., Neumann R., Faulstich F.R.L., Alves F.E.A., de Almeida F.B., Cidade T.P. and Sousa S.S.C.G. (2020) Oxycalciomicrolite, (Ca,Na)$_2$(Ta,Nb,Ti)$_2O_6$(O,F), a new member of the microlite group (pyrochlore supergroup) from the Paleoproterozoic São João del Rei Pegmatite Province, Minas Gerais state, Brazil. *Mineralogical Magazine*, **84**, 854–858.

Miyawaki R., Momma K., Matsubara S., Sano T., Shigeoka M. and Horiuchi H. (2021) Hydroxykenopyrochlore, (□,Ce,Ba)$_2$(Nb,Ti)$_2O_6$(OH,F), a new member of the pyrochlore group from Araxá, Minas Gerais, Brazil. *The Canadian Mineralogist*, **59**, 589–601.

Möller T., Clearfield A. and Harjula R. (2002) Preparation of hydrous mixed metal oxides of Sb, Nb, Si, Ti and W with a pyrochlore structure and exchange of radioactive cesium and strontium ions into the materials. *Microporous and Mesoporous Materials*, **54**, 187–199.

Momma K. and Izumi F. (2011) VESTA 3 for three-dimensional visualization of crystal, volumetric and morphology data. *Journal of Applied Crystallography*, **44**(6), 1272–1276. https://doi.org/10.1107/S0021889811038970

Philippo S., Naud J., Declercq J.P. and Feneau-Dupont J. (1995) Structure refinement and X-ray powder diffraction data for kalipyrochlore $(K,Sr,Na,Ca,H_2O)_{2-m}(Nb,Ti)_{2-x}O_{6-w}Y_{1-n}$ with ($0<m<0.8$, $x\sim0.2$, w = 0 and $0.2<n<1$). *Powder Diffraction*, **10**, 180–184.

Sheldrick G.M. (2015) Crystal structure refinement with SHELXL. *Acta Crystallographica*, **C71**, 3–8.

Slade R.C.T., Hall G.P., Ramanan A. and Prince E. (1996) Structure and proton conduction in pyrochlore-type antimonic acid: a neutron diffraction study. *Solid State Ionics*, **92**, 171–181.

Taddei A. and Bindi L. (2025) Exploring the kinetics of monovalent thallium incorporation in hydropyrochlore and hydrokenopyrochlore. *Mineralogical Magazine*, **90**, https://doi.org/10.1180/mgm.2025.10123

Taddei A., Bindi L., Lepore G.O., Skogby H. and Bonazzi P. (2024) Crystallographic insights into monovalent thallium incorporation: Exploring hydropyrochlore structure for environmental remediation. *American Mineralogist*, **109**, 1913–1920.

van Wambeke L. (1978) Kalipyrochlore, a new mineral of the pyrochlore group. *American Mineralogist*, **63**, 528–530.

Warr L.N. (2021) IMA-CNMNC approved mineral symbols. *Mineralogical Magazine*, **85**, 291–320.

Wilson A.J.C. (1992) *International Tables for Crystallography. Volume C: Mathematical, Physical and Chemical Tables*. Kluwer Academic Publishers, 900 pp.

Zoppi M. (2004) *Ossidi di Nb, Ta e Ti: processi di ricristallizzazione e relazioni cristallochimiche*. PhD dissertation, Università degli Studi di Firenze, Italy [in Italian].